Microfluid Nanofluid (2012) 12:663–669
DOI 10.1007/s10404-011-0879-1

SHORT COMMUNICATION

Ultra-sensitive, label-free probing of the conformational characteristics of amyloid beta aggregates with a SERS active nanofluidic device

Inhee Choi · Yun Suk Huh · David Erickson

Received: 29 July 2011 / Accepted: 30 August 2011 / Published online: 17 September 2011

Abstract One of the primary pathological hallmarks of Alzheimer's disease is the formation of neutric plaques in the brain. The aggregation of amyloid beta peptide (Aβ) is central to the formation of these plaques and thus trace detection and characterization of these aggregates can have significant implications for understanding and diagnosing diseases. Here we have demonstrated a label-free surface enhanced Raman scattering technique combined with nanofluidics that is able to sensitively detect Aβ aggregates and to characterize their structural and surface properties at concentrations that are much lower than the limit of detection of existing instrumentation. With our device we have successfully detected Aβ aggregates formed at a very low concentration range of 10 fM to 1 μM and shown that the extent of protein aggregation and its resulting conformational characteristics are dependent on the initial Aβ concentration. The ability to observe the early stages of the aggregation process with analytical techniques, like that demonstrated here, could help to develop a better understanding of the conditions which lead to conformational disease, such as neurodegenerative diseases.

Keywords Amyloid beta · Conformational diseases · Label-free · Nanofluidics · Protein aggregates · Raman characterization

I. Choi · Y. S. Huh · D. Erickson (✉)
Sibley School of Mechanical and Aerospace Engineering, Cornell University, 240 Upson Hall, Ithaca, NY 14853, USA
e-mail: de54@cornell.edu

I. Choi
e-mail: ic96@cornell.edu

Y. S. Huh
e-mail: ysh4@cornell.edu

1 Introduction

Alzheimer's disease (AD) is a progressive neurodegenerative disease and the leading cause of dementia in the aging population. One of the primary pathological hallmarks of AD is the formation of neutric plaques in the brain, and the aggregation of amyloid beta peptide (Aβ) is central to the formation of these plaques (Chimon and Ishii 2005; Miura et al. 2002; Thompson 2003; Fezoui and Teplow 2002; Dong et al. 2003; Inouye et al. 1993; Meier et al. 2009). Moreover, it has been hypothesized that the formation of Aβ aggregates triggers a cascade of events that brings about neuritic dystrophy and neuronal death (Chimon and Ishii 2005; Miura et al. 2002; Thompson 2003; Fezoui and Teplow 2002; Dong et al. 2003; Inouye et al. 1993). Recently, it has been reported that even low concentrations (below μM) of aggregated Aβ can bind to the neurotrophin receptor and induce abnormal signaling (Susen and Blochl 2005), and that the most prevalent conformational change in this process is an increase of β-sheet structures (Chimon and Ishii 2005; Miura et al. 2002; Thompson 2003; Fezoui and Teplow 2002; Dong et al. 2003; Inouye et al. 1993; Meier et al. 2009). Therefore, trace detection and structural probing of early stage Aβ aggregates could have an impact on understanding the molecular mechanisms behind AD.

At present, the characterization of protein structures is commonly done through circular dichroism (CD) spectroscopy (Fezoui and Teplow 2002), nuclear magnetic resonance (NMR) spectroscopy (Chimon and Ishii 2005; Baldwin et al. 2008), and X-ray crystallography (Inouye et al. 1993). Fluorescence spectroscopy combined with molecularly specific dyes, including thioflavin T (Chimon and Ishii 2005; Meier et al. 2009) and Congo red (Miura et al. 2002) has also been used to probe the formation of amyloid fibril structures. Although these methods are

functional, it is difficult to use them to detect and characterize very small amounts of Aβ aggregates. This is because Aβ does not crystallize and toxic forms of Aβ are mostly insoluble (Chimon and Ishii 2005; Thompson 2003). As we will show, these methods also lack the sensitivity required to detect trace amounts of Aβ aggregates, which limit the capability for understanding the protein conformational changes at low concentrations.

To address these problems, we have recently developed a nanofluidics-based surface enhanced Raman scattering (SERS) detection method (Choi et al. 2011) that is able to identify small amounts of protein aggregates and to simultaneously characterize their structural properties. In that earlier paper, we present proof-of-concept demonstration enabling that matured amorphous protein aggregates can be selectively concentrated at a fluidic junction and identified by label-free Raman characterization. In this study, we further utilize our method to investigate Aβ aggregation, which usually forms structurally ordered amyloid fibrils (Chimon and Ishii 2005; Miura et al. 2002; Thompson 2003; Fezoui and Teplow 2002; Dong et al. 2003; Inouye et al. 1993; Meier et al. 2009) rather than amorphous aggregates. Notably, we demonstrate that our method provides significant implication for understanding the Alzheimer's disease via elucidating protein structures at ultra-low concentration (1 fM), which is difficult to achieve with conventional methods, and can be compared with existing techniques for probing protein conformational characteristics.

2 Materials and methods

2.1 In vitro formation of protein aggregates

Amyloid β protein fragment 1–40 (Aβ (1–40), Sigma) was diluted with a phosphate buffer saline (PBS) solution at various concentrations ranging from 10 fM to 1 μM. In vitro formation of Aβ aggregates was performed by adding a 2,2,2-trifluoroethanaol (TFE) solution to the diluted SOD1 solution with TFE volume ratio (v/v) of 20%. To identify aggregate formation, each sample was added to 30 μM ThT in PBS with a volume ratio of 1:10, and ThT fluorescence of samples was measured by microplate spectrofluorometer (Gemini EM-Molecular Devices) with excitation and emission wavelengths of 435 and 480 nm, respectively.

2.2 Fabrication of a Raman active concentration device

In our device, nanofluidic channels are formed by employing our previously reported elastomeric collapse technique (Park et al. 2009). Polydimethylsiloxane (PDMS) microchannels, with a predefined aspect ratio, are first fabricated using a patterned master and traditional soft lithography processes. To begin the fabrication of the nanofluidic channels, the desired pattern was made on a silicon wafer using standard photolithography processes. Negative photoresist SU-8 (Microchem) 2000.5 (for the nanochannels) and 2010 (for the microchannels) were used to create the different heights of the master. The PDMS base to curing agent ratios were 10:1 by weight. After mixing the curing agent and elastomer base and degassing the mixture, it was cast onto the premade master and allowed to cure at 80°C for 4 h. After the PDMS mold was removed from the master, it was bonded to a SERS active substrate by plasma oxidation for 30 s. The SERS active substrate was prepared by immobilizing 80 nm gold nanoparticles onto the 3-aminopropyltrimethoxysilane (APTMS)-modified glass slide, which was made from the molecular vapor deposition (MVD 100).

2.3 Micro/nanofluidic concentration

Our experiments were carried out after sampling from protein solutions, which were incubated in vitro outside the device. Aβ aggregation occurred in free solution and samples were taken periodically (0 day, 2 days, 1 week, and 2 months) for analysis. The devices were operated by simple pressure driven injection of sample solutions. This operation was completed in less than 1 h. Considering that aggregation process in vivo as well as in vitro is quite slow compared with the analysis time, it is expected that there is no significant further aggregation during chip operation.

2.4 Raman spectroscopy

Raman measurements were performed using a Renishaw inVia Raman microscope spectrometer coupled to a Leica microscope by focusing the excitation laser on the concentrated sample. The 785 nm laser was used as optical excitation source and the scattered signal was collected by a Peltier-cooled CCD detector. A 20× (NA = 0.40) objective lens was used to focus the laser beam spot onto the sample surface. Each Raman spectrum was collected by averaging three consecutive scans. The spectra in the 800–1,700 cm^{-1} region were examined here. Each figure showing multiple spectra has been artificially offset for visual clarity of the figure with baseline correction.

2.5 Circular dichroism (CD) spectroscopy

The secondary structures of Aβ aggregates were determined by CD analysis (Aviv 400 Circular Dichroism Spectrometer). A 0.1-cm quartz cell was used for the measurements and the CD spectra were recorded from 190

to 260 nm. All CD measurements were carried out using the following parameters: 1 nm bandwidth, 30 nm/min run speed, and an average of three runs.

3 Results and discussion

Figure 1 is a schematic that illustrates the used devices here. In short, the device (Fig. 1a) is composed of micro/nanofluidic junctions (Fig. 1b) and a gold nanoparticle based SERS-active surface (Fig. 1c). The Aβ aggregates of interest here are generally observed in the form of amyloid fibrils, which have nanometer scale diameters and micrometer scale lengths (Chimon and Ishii 2005; Miura et al. 2002; Thompson 2003; Fezoui and Teplow 2002; Dong et al. 2003; Inouye et al. 1993; Meier et al. 2009). Due to this large aspect ratio, they can be trapped at the junction between the microchannel and the nanochannel. Prior to final assembly, the micro/nanofluidic junction is aligned with the immobilized gold nanoparticle clusters,

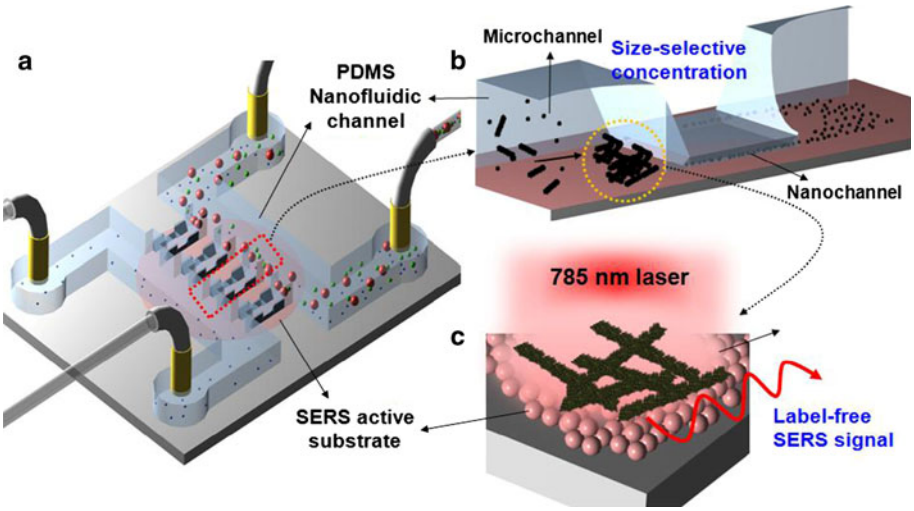

Fig. 1 Schematic of the procedure for the concentration and characterization of Aβ aggregates. **a** Overall description of SERS active nanofluidic device. **b** The fluidic junction between the microchannel and the nanochannel used for size-selective concentration. **c** Close up view of Aβ aggregates concentrated near the gold nanoparticle-immobilized substrate used for label-free SERS detection

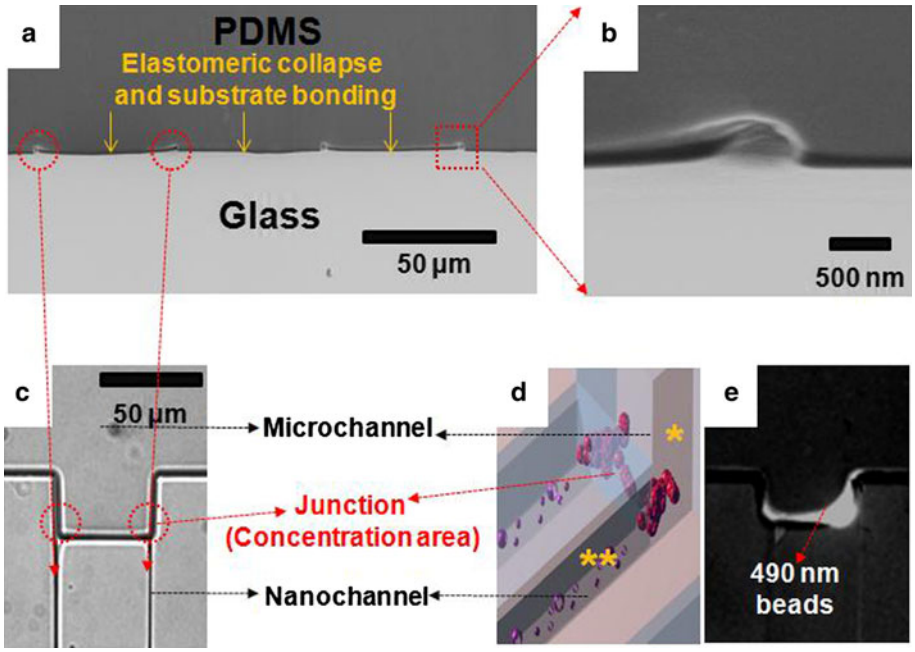

Fig. 2 Details of the nanofluidic concentration device used here. **a** SEM images of a cut plane though the fabricated nanochannels by elastomeric collapse. **b** A magnified image of the nanochannel. **c** Top view of nanofluidic channels formed by PDMS collapse. **d** Tilted side view of three dimensional schematic showing the size-selective concentration process at the junction between microchannel (*asterisk*) and nanochannel (*double asterisk*). Large molecules accumulate at this fluidic junction, while small molecules pass through the junction. **e** *Fluorescent image* of 490 nm polystyrene beads accumulated at the junction between a microchannel and a nanochannel

which serves as the Raman enhancer, on the bottom substrate. To assemble the final device, the PDMS mold with a predefined aspect ratio was placed onto the gold nanoparticle clusters and allowed to form micro/nanofluidic junctions by elastomeric collapse (Park et al. 2009). As shown in Fig. 2a–c, the width of the fabricated nanochannel was below 500 nm and its height was smaller than its width. The approximate dimensions of the final collapsed nanochannel were determined by testing the size-selective trapping performance (Fig. 2d) with different sized beads (51 nm, 210 nm, and 490 nm). Using hydrodynamic sample injection, 490 nm beads were accumulated at the fluidic junctions (Fig. 2e), while 51 and 210 nm beads passed through the channel.

Using this device, we first investigated Aβ aggregation as a function of incubation time. Aβ aggregates were prepared by the treatment of Aβ (1–40) fragments (which represent the most prevalent form of Aβ) with 2,2,2-trifluoroethanol (TFE), which has been extensively used to study the aggregation of other proteins (Fezoui and Teplow 2002; Calamai et al. 2005; Stathopulos et al. 2003; Yamaguchi et al. 2005). To visualize the size-selective concentration performance for the matured Aβ aggregates, the incubated Aβ were treated with thioflavin T (ThT), a common dye traditionally used to monitor the formation of protein aggregates (Chimon and Ishii 2005; Meier et al. 2009) before injection. As shown in Fig. 3, with increasing incubation time, the amount of Aβ aggregates accumulated at the fluidic junction also increases, consistent with the expected existence of greater number of aggregates with sizes over the width and height of the nanochannel. No significant concentration at the junction was observed at the initial state, as the expected structures comprised primarily of small Aβ variants and not matured aggregates.

To demonstrate the enhanced limit of detection achievable via nanofluidic concentration, we performed a series of Aβ aggregation detection experiments with initial concentration ranging from 10 fM to 1 μM and compared with traditional fluorescence spectroscopy. As shown in Fig. 4a, Aβ aggregates were observed at the concentration junction even at the very lowest concentration (10 fM), while the standard fluorescence technique was not capable

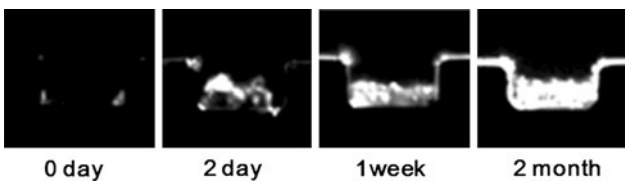

Fig. 3 Size-selective concentration of Aβ aggregates. Aβ aggregates were prepared with different incubation times (2 months, 1 week, 2 days, and 0 days). *Fluorescent images* show the Aβ aggregates concentrated at the micro/nanofluidic junctions

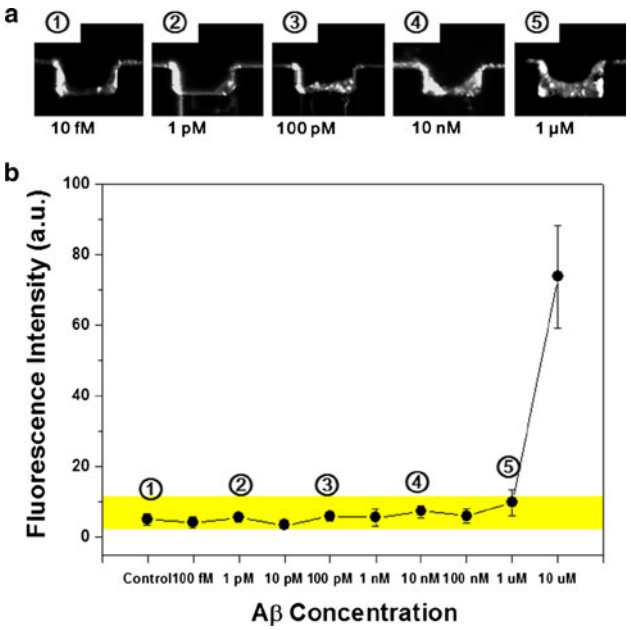

Fig. 4 Quantitative analyses of concentration-dependent Aβ aggregation: comparison of fluorescence signals obtained from nanofluidic device with traditional fluorescence analysis. **a** With the nanofluidic device: each sample solution with volume of 10 μl was injected into a nanofluidic device and then the concentrated protein aggregates were observed by imaging with fluorescence microscopy. **b** Traditional fluorescence analysis: each sample solution with volume of 200 μl was added into a well in a 96-microwell plate, and then fluorescence intensities were measured by fluorescence spectroscopy. The *highlighted band* of the graph indicates the range of intensities measured for the concentrations examined with our device

of detecting Aβ aggregates at concentrations below 10 μM (see Fig. 4b). This can be attributed to the ability of our device to directly collect Aβ aggregates in the confined area to be measured. Note that insolubility of Aβ aggregates and their non-uniform distribution in solution can result in an inaccurate measurement in the case of other solution-based analysis techniques (i.e., fluorescent spectroscopy and CD spectroscopy).

To structurally probe the conformational changes of Aβ incubated at different concentrations, we further collected Raman spectra (Fig. 5a) from our device and compared the results with conventional CD spectroscopy (Fig. 5b). At 10 μM, the CD spectrum shows the characteristic peak for β-sheets. As can be seen, the intensity of this peak drastically decreases around 1 μM and is indistinguishable below 10 nM. The Raman spectra show the clear signatures for concentrated Aβ aggregates irrespective of the initial concentrations (more than 100 pM). The structural significance of the observed Raman bands was identified on the basis of existing literature pertaining to the spectra of amino acids and proteins (Chen et al. 2009; Dong et al. 2003; Lednev et al. 2009; Maiti et al. 2004; Chou et al. 2008). Table 1 summarizes the relevant Raman bands observed here. Since

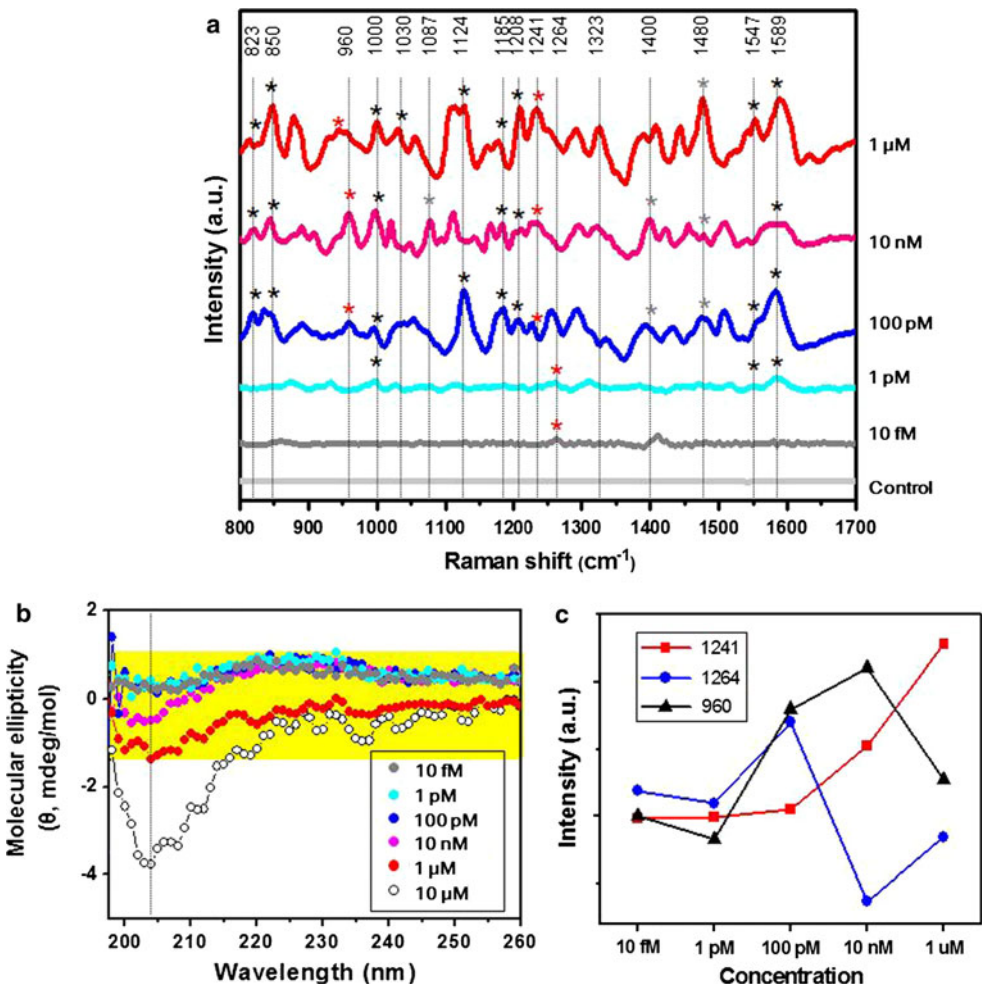

Fig. 5 Structural analyses of concentration-dependent Aβ aggregation: correlation of SERS technique combined with a nanofluidic device and traditional CD analysis. **a** SERS spectra obtained from SERS active nanofluidic device. **b** CD spectra, a *highlighted band* indicates the concentration range examined in **a**. **c** A plot for concentration dependent relative intensity at several peaks, which were closely associated with the secondary structures (1,241 and 1,264 cm^{-1}) and surface properties (960 cm^{-1}), in SERS spectra of **a**

Raman signatures tend to depend on the extent of protein aggregation and its resulting conformation, here we focus on the interpretation of the most compelling changes (i.e., secondary structures and surface hydrophobicity, indicated with red asterisks in Fig. 5a) in proteins during the aggregation process. Variations in the amide III region (1,200–1,300 cm^{-1}) reflect the changes in secondary structures and are widely used to quantitatively explore the components of β-sheet structure (around 1,240 cm^{-1}) and α-helix structure (around 1,260 cm^{-1}). Additionally, the increase of the band at 960 cm^{-1} (assigned to the C–C stretching in the hydrophobic segment of polypeptide backbone) can be attributed to the increase of hydrophobicity of protein surface, since the conformational changes in proteins are generally accompanied by structural turnover and changes in surface residues. In Fig. 5a, peaks indicated with black asterisks are related to hydrophobic residues (i.e., phenylalanine, valine, and isoleucine) and gray asterisks indicate charged and hydrophilic residues (i.e., lysine, arginine, glutamine, asparagine, aspartic acid, glutamic acid, and histidine).

At both 10 fM and 1 pM, a band in the amide III region, close to 1,260 cm^{-1}, was detected which reveals the existence of partially folded α-helix containing intermediates at a low concentration. As the concentration increased, numerous other features can be observed in the Raman spectra. In particular, the systemic increase of the band at 1,241 cm^{-1} and the fluctuation of a band at 1,264 cm^{-1} (Fig. 5c) indicate that Aβ monomers are aggregated to β-sheet abundant structures under destabilizing conditions by the formation and consumption of α-helix containing intermediates. This finding is consistent with many reports (Fezoui and Teplow 2002; Lednev et al. 2009) suggesting that the partially folded intermediate is prone to aggregation, and its native-like secondary structure is converted to an extended β-sheet structure during this process. Above a concentration of 100 pM, the 1,264 cm^{-1} band is hidden in the spectrum. This is a good indication that main polypeptide backbones of Aβ aggregates begin to possess matured β-sheet rich fibrils rather than helical intermediates. Moreover, a large number of bands associated with hydrophobic residues become more prominent. This is also

Table 1 Assignment of bands in SERS spectra of Aβ aggregates

Wavenumber (cm^{-1})	Assignment	Comment
823	Tyr doublet	Hydrophobic
850	Tyr	Hydrophobic
960	n(C–C)	Hydrophobicity
1,000	Phe	Hydrophobic
1,030	Phe	Hydrophobic
1,087	Lys, Arg, Gln, Asn	Charged (+)
1,124	Val and Ile	Hydrophobic
1,185	Phe and Tyr	Hydrophobic
1,208	Phe and Tyr	Hydrophobic
1,241	Amide III (β-sheet)	β-sheet structure
1,264	Amide III (α-helix)	α-helix structure
1,323	Amide III and CH_2 twist/wag	Amide III
1,400	Asp, Glu, υ(COO−)	Charged (−)
1,480	His	Charged (+)
1,547	Phe	Hydrophobic
1,589	Phe	Hydrophobic

Tyr tyrosine, *Phe* phenylalanine, *Lys* lysine, *Arg* arginine, *Gln* glutamine, *Asn* asparagine, *Val* valine, *Ile* isoleucine, *Asp* aspartic acid, *Glu* glutamic acid, *His* histidine

directly correlated with the increase of a band at 960 cm^{-1} (Fig. 5c), which reflects the insoluble property of Aβ aggregates (Chimon and Ishii 2005; Thompson 2003). We note here that the structural investigation of Aβ aggregation at these low concentrations is difficult with using conventional CD spectroscopy (in a highlighted box in Fig. 5b).

4 Conclusions

In conclusion, we have investigated and elucidated Aβ aggregation and its structural evolution at concentrations much lower than what is achievable with standard instrumentation, using our label-free SERS active nanofluidic device. We have used this device to investigate a series of aggregation procedures including the formation, consumption of α-helix containing intermediates, and growth to β-sheet abundant structures at concentrations ranging from very low (10 fM) to relatively high (1 μM). In Raman spectra, analysis of protein amide III band profiles provided information on the composition of secondary structures (α-helix and β-sheet), and some bands revealed several sensitive markers of the exposed protein surface residues. As a result, we can comprehensively understand the surface and structural properties of the protein aggregates according to their aggregation stage at very low concentrations.

Acknowledgments The authors acknowledge funding from and access to the facilities of the Nanobiotechnology Center (NBTC), an STC Program of the National Science Foundation under Agreement no. ECS-9876771. The authors also appreciate access and use of the Cornell Nanoscale Science and Technology Facility, which is supported by the National Science Foundation under grant ECS-9731293. I. Choi was partially supported by a grant from the National Research Foundation of Korea Grant funded by the Korean Government [NRF-2009-352-D00053].

References

Baldwin AJ, Anthony-Cahill SJ, Knowles TPJ, Lippens G, Christodoulou J, Barker PD, Dobson CM (2008) Measurement of amyloid fibril length distributions by inclusion of rotational motion in solution NMR diffusion measurements. Angew Chem Int Ed 47(18):3385–3387

Calamai M, Canale C, Relini A, Stefani M, Chiti F, Dobson CM (2005) Reversal of protein aggregation provides evidence for multiple aggregated states. J Mol Biol 346(2):603–616

Chen P, Shen AG, Zhao W, Baek SJ, Yuan H, Hu JM (2009) Raman signature from brain hippocampus could aid Alzheimer's disease diagnosis. Appl Opt 48(24):4743–4748

Chimon S, Ishii Y (2005) Capturing intermediate structures of Alzheimer's beta-amyloid, A beta(1–40), by solid-state NMR spectroscopy. J Am Chem Soc 127(39):13472–13473

Choi I, Huh YS, Erickson D (2011) Size-selective concentration and label-free characterization of protein aggregates using a Raman active nanofluidic device. LChip 11:632–638

Chou IH, Benford M, Beier HT, Cote GL, Wang M, Jing N, Kameoka J, Good TA (2008) Nanofluidic biosensing for beta-amyloid detection using surface enhanced Raman spectroscopy. Nano Lett 8(6):1729–1735

Dong J, Atwood CS, Anderson VE, Siedlak SL, Smith MA, Perry G, Carey PR (2003) Metal binding and oxidation of amyloid-beta within isolated senile plaque cores: Raman microscopic evidence. Biochemistry 42(10):2768–2773

Fezoui Y, Teplow DB (2002) Kinetic studies of amyloid beta-protein fibril assembly—differential effects of alpha-helix stabilization. J Biol Chem 277(40):36948–36954

Inouye H, Fraser PE, Kirschner DA (1993) Structure of beta-crystallite assemblies formed by Alzheimer beta-amyloid protein analogues: analysis by X-ray diffraction. Biophys J 64(2):502–519

Lednev IK, Shashilov V, Xu M (2009) Ultraviolet Raman spectroscopy is uniquely suitable for studying amyloid diseases. Curr Sci 97(2):180–185

Maiti NC, Apetri MM, Zagorski MG, Carey PR, Anderson VE (2004) Raman spectroscopic characterization of secondary structure in natively unfolded proteins: alpha-synuclein. J Am Chem Soc 126(8):2399–2408

Meier M, Kennedy-Darling J, Choi SH, Norstrom EM, Sisodia SS, Ismagilov RF (2009) Plug-based microfluidics with defined surface chemistry to miniaturize and control aggregation of amyloidogenic peptides. Angew Chem Int Ed 48(8):1487–1489

Miura T, Yamamiya C, Sasaki M, Suzuki K, Takeuchi H (2002) Binding mode of Congo Red to Alzheimer's amyloid beta-peptide studied by UV Raman spectroscopy. J Raman Spectrosc 33(7):530–535

Park SM, Huh YS, Craighead HG, Erickson D (2009) A method for nanofluidic device prototyping using elastomeric collapse. Proc Natl Acad Sci USA 106(37):15549–15554

Stathopulos PB, Rumfeldt JAO, Scholz GA, Irani RA, Frey HE, Hallewell RA, Lepock JR, Meiering EM (2003) Cu/Zn superoxide dismutase mutants associated with amyotrophic lateral sclerosis show enhanced formation of aggregates in vitro. Proc Natl Acad Sci USA 100(12):7021–7026

Susen K, Blochl A (2005) Low concentrations of aggregated beta-amyloid induce neurite formation via the neurotrophin receptor p75. J Mol Med 83(9):720–735

Thompson LK (2003) Unraveling the secrets of Alzheimer's beta-amyloid fibrils. Proc Natl Acad Sci USA 100(2):383–385

Yamaguchi K, Takahashi S, Kawai T, Naiki H, Goto Y (2005) Seeding-dependent propagation and maturation of amyloid fibril conformation. J Mol Biol 352(4):952–960